

# 2-D Finite-Element Electromagnetic Analysis of an Autotransformer Experiencing Ferroresonance

Charalambos A. Charalambous, *Member, IEEE*, Zhongdong D. Wang, *Member, IEEE*, Paul Jarman, and Mark Osborne

**Abstract**—The key concern for transformers experiencing ferroresonance is whether the energy transferred into the transformer body during core saturation by the nonsinusoidal currents is damaging. Saturation and the consequent incompetency of the core to contain the flux manifests itself as current induced in parts of the transformer body not foreseen to conduct current. Sustained ferroresonance may last for minutes (or even hours), when no intervening operations are carried out, and may cause local overheating and thermally degrade surrounding insulation. In this paper, transient electromagnetic analysis was conducted by using 2-D finite-element models of a 240-MVA 400/132/13-kV autotransformer. As a continuing effort, the main objective of modeling is to visualize the flux flow in parts where transformer designers have not anticipated its presence. A quantitative assessment of the flux, the induced currents, and the power dissipated in these parts has been carried out to determine the degree of risk imposed on a transformer under ferroresonance.

**Index Terms**—Failure mechanisms, ferroresonance, finite elements, transformers.

## I. INTRODUCTION

**F**ERRORESONANCE is a low-frequency phenomenon that may occur in a power transformer when one side of a double-circuit transmission line connected to the transformer is switched out. The transfer of power from the adjacent energized line through capacitive coupling into the de-energized line could excite the unloaded transformer. As a result, the overfluxing of the transformer leads to lasting ferroresonant voltages and currents, stressing the disconnectors during isolation and more typically affecting control and protection functions. The worst-case scenario associated with ferroresonance would be to prevent circuit operations and possibly require unplanned double-circuit outages to safely isolate the distressed transformer [1], [2].

The mitigation of ferroresonance has been a subject of research in the past decades [3]–[5]. Specifically, in the U.K., the

Manuscript received May 13, 2008; revised November 17, 2008. First published April 28, 2009; current version published June 24, 2009. This work was supported part by National Grid plc U.K. Paper no. TPWRD-00351-2008.

C. A. Charalambous and Z. D. Wang are with the School of Electrical and Electronic Engineering in the University of Manchester, Manchester, M60 1QD, U.K. (e-mail: charalambos.charalambous@manchester.ac.uk; zhongdong.wang@manchester.ac.uk).

P. Jarman and M. Osborne are with the Asset Strategy Group, National Grid, Warwick CV34 6DA, U.K. (e-mail: paul.jarman@uk.ngrid.com; mark.osborne@uk.ngrid.com).

Color versions of one or more of the figures in this paper are available online at <http://ieeexplore.ieee.org>.

Digital Object Identifier 10.1109/TPWRD.2009.2016629

relay for ferroresonance detection looks for a voltage ratio of 2:1:1 (fundamental mode—50 Hz), as would be theoretically expected for the worse case [6]. However, in some situations, the voltage ratio may vary away from 2:1:1, especially for the subharmonic mode case of 16 2/3 Hz. This may lead to the detection system failing to recognize ferroresonance and consequently, the transformer core could stay in saturation for a long period of time; increasing the thermal duty of the transformer insulation. Alternatively, evidence of the ferroresonance occurrence could be the Bucholtz alarm/relay, which indicates oil gassing/faults. However, the Bucholtz alarm, following transformer ferroresonance, would indicate that damage had already occurred in the transformer and, therefore, it is not acceptable as a preferred detection method.

Over the years, ferroresonance research activities, besides establishing mitigation measures, have also concentrated their efforts to predict or confirm ferroresonance occurrence in susceptible networks. The latter primarily pertains to mathematically adequate transformer models for computer transient simulations [7], [8]. Nevertheless, the complexity of a transformer's geometrical structure still poses a challenge for researchers to understand the flux redistribution during core saturation and the consequent transformer failure mechanism. It is the authors' understanding and experience that sustained, periodic, and high-magnitude ferroresonant currents give rise to a high magnetomotive force (MMF) which not only corresponds to core saturation but also causes flux to escape from the core and penetrate other structural parts which are either normally shielded by the core steel or separated by an insulating gap sufficient to ensure that the leakage fields under normal excitation decay to a negligible level.

While a number of wound voltage transformers have failed due to ferroresonance [1], power transformers directly associated with ferroresonance have reportedly not failed. Nonetheless, it is still believed that ferroresonance is a contributing factor to the eventual failure modes by exposing the transformer's components to electromagnetic (EM) and thermal stresses. The impact on these components could mainly be attributed to accelerated aging and can be estimated through the power dissipated through ohmic heating.

For the purpose of this paper, the authors have quantified ferroresonant currents for a 240-MVA 400/132/13-kV autotransformer, based on their work conducted in the past [9], [10]. These ferroresonant currents were used as excitation inputs to 2-D finite-element transient EM models of the transformer. The main objective of this paper rests in the continuing efforts to

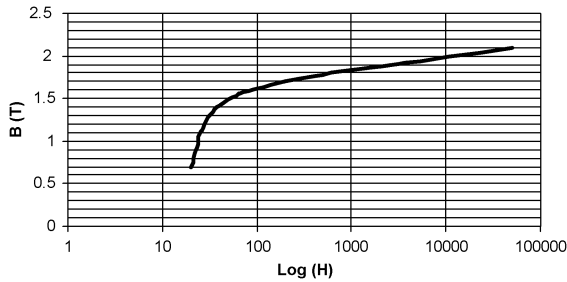
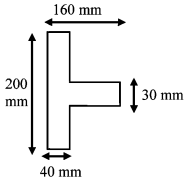


Fig. 1. Electrical steel unisil 35M6 characteristic.

TABLE I  
DIMENSIONS AND MATERIAL PROPERTIES OF PARTS

Parts	Dimensions	Material	Properties
Tank	Thickness 12mm for wall and 20 mm for lid	Mild steel	B-H curve (material defined) $\sigma = 6.0 \text{ MS/m}$
T- Core frame			
Core bolts	25 mm diameter		
Flux shunt	50mm (H)×400mm (W)	Unisil 35M6	$\sigma = 2.0833 \text{ MS/m}$

visualize the flux escape, during core saturation, into the regions and components other than the core. The losses induced in these parts (i.e., core bolts, flux shunts, and core frames) are calculated.

## II. CHARACTERISTICS OF 240-MVA AUTOTRANSFORMERS

The 240-MVA 400/132/13-kV autotransformer of the National Grid has a five-limb core manufactured from transformer steel Unisil 35M6 with a stacking factor of 0.97. Fig. 1 illustrates the material's characteristic curve on a semilog plot. The operating flux density is designated to be 1.61 T. In the test report, it is stated that under nominal voltage, the magnetizing current is measured at the 400-kV side as 0.3 A rms.

The transformer is physically constructed with four concentric windings for each phase (i.e., tertiary, tap, common, and series windings, taken outwards from the core). The physical dimensions of the structure (i.e., core limb and yoke, winding, insulation clearance, and other structural parts) were available from the manufacturer's design data. The dimensions of the parts under specific study in this paper and their relevant material properties are tabulated in Table I.

## III. QUANTIFICATION OF FERRORESONANT CURRENTS

Power transformer ferroresonance conditions are illustrated diagrammatically in Fig. 2. An energized adjacent line (on a double-circuit tower) is capable of supporting an established ferroresonance condition, which may arise between the nonlinear

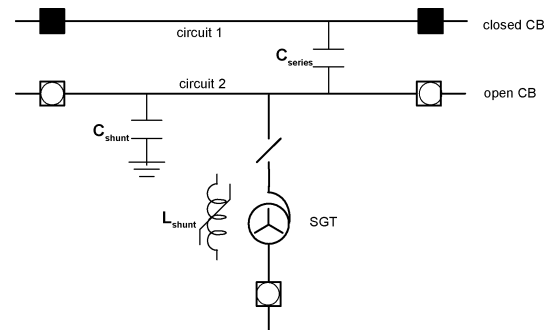


Fig. 2. Typical circuit configuration which can exhibit ferroresonance.

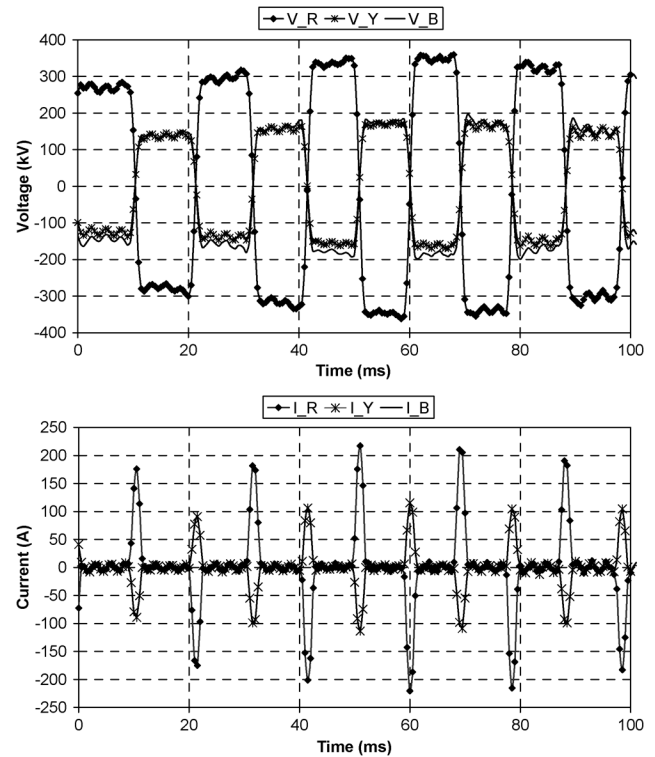


Fig. 3. Fundamental mode ferroresonance—phase voltages and line currents.

inductance of the transformer and the de-energized line-circuit capacitance to ground.

References [11]–[14] have proposed a variety of nonlinear transformer core models for ferroresonant studies. Nonetheless, model validations using real-scale test results during switching operations at 400-kV system networks are rarely reported, except in [1], [9], and [10].

Fig. 3 shows the line currents and the phase voltages produced by simulation under the sustained fundamental mode ferroresonance. It is noted that from the time of circuit-breaker (CB) opening to the time steady-state ferroresonance voltages become sustained, there is a transition period where switching transient and oscillatory voltages occur. The occurrence of the sustained fundamental mode or the sustained subharmonic-mode ferroresonance is highly sensitive to the switching times and the losses of the circuit.

National Grid experience suggests that the sustained fundamental mode of ferroresonance is the most severe case due to the high energy transferred to the transformer. For the purpose of

this study, various switching operations were simulated to quantify the maximum sustained ferroresonant voltages and currents of the transformer.

In the finite-element simulation, a small time step is necessary in order to accurately model the rapidly changing waveform. Unfortunately, the field measurements of voltage and current were made only every 1 ms, too crude for use directly in the finite-element calculation. Instead, they were used to validate an equivalent-circuit-based simulation of a ferroresonance condition whose output was fine enough to be suitable for use in the finite-element calculation.

#### IV. FINITE-ELEMENT MODELING

##### A. Approximations When Using a 2-D Model

A literature survey reveals that 2-D finite-element models have been extensively used in assessing fault conditions in electrical machines [16]–[18] and in assessing the effects of geomagnetically induced currents (GICs) on power transformers [19]. However, it should be kept in mind that 2-D models require some approximations to represent the EM behavior of the transformer components. In fact, only 3-D models can accurately represent the topological arrangement of transformer components and consequently their EM behaviours. Although these 3-D models can be built within the slim FEA software [20] of AREVA T&D, the calculation of the transient time-domain solution, particularly multiple cases or conditions, is restricted by the current computational power. Therefore, presently, any transient time-domain analysis is limited to 2-D models.

The authors have utilized a combination of two 2-D models, namely, the axisymmetric model (Fig. 4) and the transverse view model (Fig. 5), to carry out their analysis. The fundamental logic of this approach is that these two 2-D models can respectively complement each other's limitations, as will be further discussed, enabling a combined 2-D analysis. Specifically, the transverse view model is used to establish the level of core saturation under ferroresonance conditions. This information (encapsulated in the value of the core permeability) is then transferred to the axisymmetric model, in which the effects of the leakage field are calculated.

Bearing in mind that one of the objectives of this study is to determine the losses induced during core saturation in parts other than the core, an axisymmetric model is considered to be an appropriate choice. Fig. 4 illustrates the top quadrant of the 2-D axisymmetric view of one main limb of the five-limb core. The core, winding, tank, core bolts, flux shunts, and core frames are topologically accurately represented. However, a disadvantage of this model is that it cannot represent the other two phases of winding and the other four limbs of the core (five limbs in total) and, hence, cannot introduce the flux flow perpendicular to the model—along the yoke or along the flux shunt or core frame from limb to limb. The model also assumes that all of the components are cylindrical, which is particularly true for windings and core limbs but deviates from reality for the tank, core frames, and flux shunts.

Since the problem is approached in 2-D, an alternative view, such as the 2-D transverse view, can be introduced in conjunction with the axisymmetric model. Fig. 5 illustrates the top half

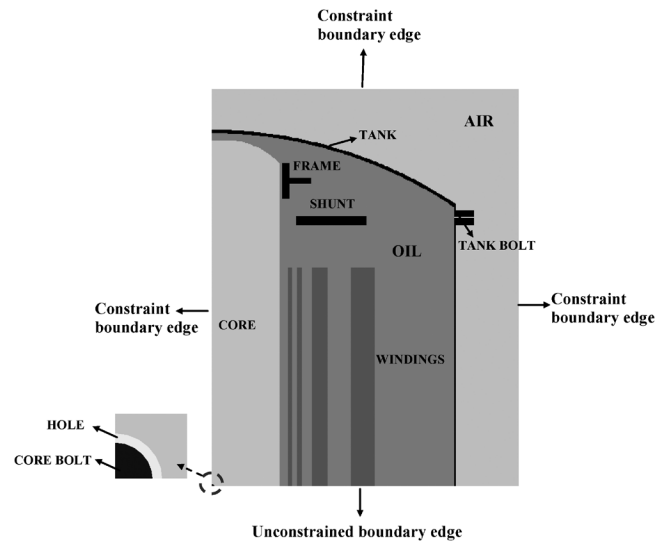


Fig. 4. Axisymmetric view of the transformer FEM.

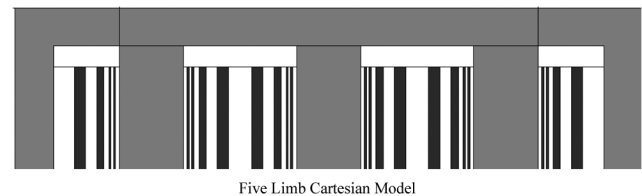


Fig. 5. Transverse view of the transformer FEM.

of the transverse view of the five-limb three-phase transformer. The transverse view can accurately represent the flow of flux from limb to limb and from phase to phase. There is, however, no mechanism for including the core frames or shunts, nor the tank at its closest proximity to the windings in front of and behind the view of Fig. 5.

The magnetostatic and transient studies on the transverse view model, as will be presented in Section V, have formed the means to understand the flux distribution under ferroresonance. The conclusions from these studies will therefore facilitate the transient solution of the 2-D axisymmetric model as will be further discussed.

##### B. Boundary Conditions

In both models, symmetry conditions were implied on the bottom half (Fig. 5) and the other three quadrants (Fig. 4) to reduce the mesh size and solution time. When symmetry conditions are applied [21], various boundary conditions can be considered. The lower horizontal boundary edge of the models in Figs. 4 and 5 were left unconstrained. In a magnetic vector potential solution, the unconstrained boundary edge implies mirror symmetry across this edge. In this way, the equipotential contours of magnetic vector potential will cross the unconstrained edge perpendicularly. This will ensure continuity of the flux in the limb. Furthermore, the other edges of models in Figs. 4 and 5 were constrained to a value of zero magnetic potential, implying that no flux will cross those boundary edges.

### C. Finite-Element Mesh

The discretization of the meshes needs to be consistent with a reasonable solution time, with smaller elements at the inner surface of the components where the field changes most rapidly. In particular, with reference to Fig. 4, the skin effect was modelled by subdividing the mesh at the tank inner and core bolt outer surfaces to 0.25 mm (the skin effect for steel is approximately 1 mm). The discretization of the mesh was designed to enable the elemental loss (concentrated at the inner tank surface due to skin effect) to be modelled as accurately as possible.

### D. 2-D Finite-Element Model Calculations

The software calculates the winding flux linkage by utilizing the vector magnetic potential, expressed in webers per meter—flux divided by the length in the direction of the vector component considered and the current component producing it. The windings are treated as current sources and are assumed to be sufficiently finely stranded and transposed so that no eddy currents are induced in them. The relationship between the winding flux linkage and average vector potential is given in [23]. The magnetic vector potential  $\underline{A}$  (in webers per meter) is related to the flux density by

$$\nabla \times \underline{A} = \underline{B}. \quad (1)$$

This expands to

$$B_x = \left[ \frac{\partial A_z}{\partial y} - \frac{\partial A_y}{\partial z} \right] \quad B_y = \left[ \frac{\partial A_x}{\partial z} - \frac{\partial A_z}{\partial x} \right] \quad B_z = \left[ \frac{\partial A_y}{\partial x} - \frac{\partial A_x}{\partial y} \right] \quad (2)$$

where  $A_z$  is then a measure of flux circulating in the  $x$ - $y$  plane per unit length in the  $z$  direction.

Although  $\underline{A}$  is a vector quantity in 3-D, it can be conveniently reduced to a scalar quantity in the 2-D models since a current, which is assumed to only flow in the  $z$ -direction, produces  $A$  (vector potential) in  $z$  direction, and  $x$  and  $y$  components of the  $B$ -flux density.

That is

$$J = kJ_z \quad \text{and} \quad A = kA_z. \quad (3)$$

From

$$\nabla \times \underline{H} = \underline{J} \quad \text{and} \quad \nabla \cdot \underline{B} = 0 \rightarrow \frac{\partial B_x}{\partial x} + \frac{\partial B_y}{\partial y} + \frac{\partial B_z}{\partial z} \quad (4)$$

the Poisson equation in 2-D for the magnetic vector potential in terms of the source current density, the material properties, and the variation through space are derived. This equation is solved in numerical form by the finite-element method

$$J_z = -\frac{1}{\mu_o \mu_r} \left[ \frac{\partial^2 A_z}{\partial x^2} + \frac{\partial^2 A_z}{\partial y^2} \right]. \quad (5)$$

Furthermore, within the 2-D magnetic-field solvers employed, stacking factors are utilized to modify permeability values in the three Cartesian directions. The user specifies values of relative permeability for linear materials or BH data files for nonlinear materials. Consequently, the directional anisotropy in the core is modeled via stacking factors [24]. For the purpose of this study, the stack factors utilized are  $sf_x = 1$ ,  $sf_y = 1$ , and  $sf_z = 0.97$  for the  $x$ - $y$ - $z$  directions, respectively.

It should be noted, however, that the directional permeabilities will not significantly influence the leakage flux and in the case they are ignored, this will give a pessimistic result.

In high-frequency power transformer modeling, more specifically in [25], the authors have used a complex permeability for representing transformer steels. However, they show that for a M6 lamination, at low frequencies, the ratio between real (inductance) and imaginary (resistance) of the equivalent complex permeabilities is significantly higher than that at high frequencies. It should be reiterated at this point that ferroresonance is a low-frequency phenomenon and most important, this case study predominantly deals with 50-Hz ferroresonance waveforms. Since ferroresonance is a low-frequency effect, iron losses in the laminations can be modeled satisfactorily by using the manufacturer's curves, as this paper suggests, and the effect that they will have on the flux distribution can be ignored.

### E. Solution Mechanism

The time-domain magnetic 2-D solver works by performing a transient solution at each point in time, utilizing the excitation data corresponding to that specific time instant.

The induced currents are calculated from the differences between the magnetic vector potentials of the present time step and the previous time step. If there were no conducting materials, this process would reduce to a series of magnetostatic solutions without mechanism or necessity to link them. It is the presence of induced currents which causes the transient behavior and requires the current solution to depend on the previous ones.

## V. STUDIES ON 2-D TRANSVERSE VIEW MODEL

### A. Magnetostatic Studies

As a mean to explore the flux in the core under the extreme excitation conditions, the transverse view transformer model in Fig. 5 was first calibrated under the normal magnetizing condition by performing magnetostatic studies. For these magnetostatic studies, the tank was not modeled explicitly, but instead was represented by a constrained (flux line) boundary. This constraint boundary would not allow any flux to escape beyond the tank inner surface; this is an important approximation when considering the magnetic conditions in the core.

The 50-Hz magnetising current of 0.3 A rms at the 400-kV side would produce a peak flux density of 1.61 T, according to the test reports. The finite-element model produced a peak flux density of 1.71 T instead of 1.61 T. This discrepancy was due to the fact that the model ignored all of the small gaps at the joints of the core laminations, which are unavoidable during core manufacture. To align the model with the practical condition of the manufactured core, a modelling trick was applied. The magnetic field strength— $H$  values of the  $B$ - $H$  characteristics of Unisil 35M6 were scaled by 1.375 times. Stretching the  $B$ - $H$  curve in this way incorporates the effect of the air gaps (equivalent to step-lapped joint) inserted across the yokes and outer limbs, and is one way of calibrating the overall reluctance of the core model.

Fig. 6 illustrates the time modulus of the flux density distribution in the five-limb core model at the zero phase angle under normal magnetizing conditions. Phase R is the reference

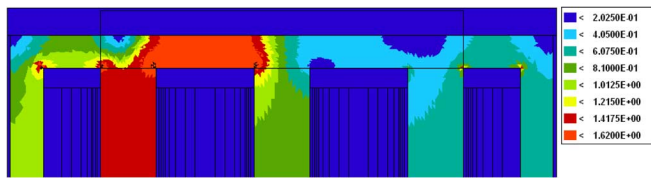


Fig. 6. Flux density (Tesla) in the model under normal magnetizing currents—magnetostatic study.

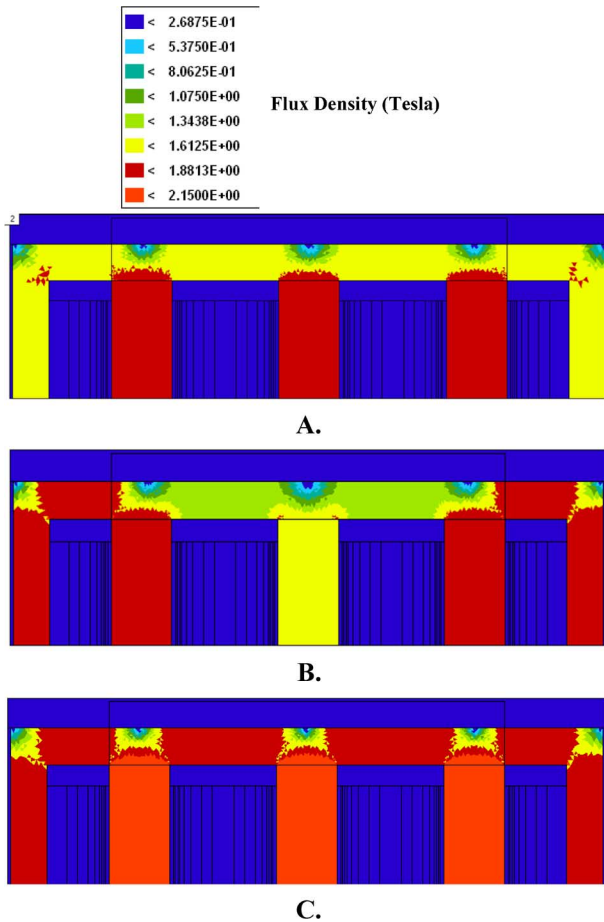


Fig. 7. Flux density in the model under ferroresonant currents—transient magnetic studies. (a) Flux density—transient magnetic study –1 ms. (b) Flux density—transient magnetic study –5 ms. (c) Flux density—transient magnetic study –10 ms.

phase. It is noted that the core flux density was further verified by performing a time domain solution—injecting a time domain three-phase magnetizing current (0.3 A).

*B. Transient Studies*

For *Y*-connected 400-kV windings, the line current is the same as the phase current; the ferroresonant current waveforms of Fig. 3 were used to provide excitation, the amp-turn product on the 400-kV winding, for the transient studies of the model in Fig. 5.

Fig. 7 illustrates the core flux density distribution at different instants of ferroresonance. In all cases, the core limbs and yokes have high flux densities and tend to saturate partly or wholly. Specifically, at 10 ms, where all three phases’ ferroresonant currents are at their peak values as shown in Fig. 3, all five limbs

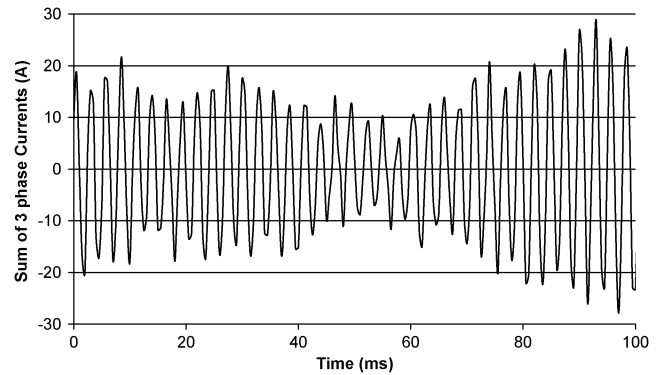


Fig. 8. Zero-sequence currents during ferroresonance  $3I_0 = I_R + I_Y + I_B$ .

of the core are highly saturated as shown in Fig. 7(c). The subplots A and B of Fig. 7 also illustrate evidence of saturation at the majority of the core limbs. The calculated core flux density indicates that the highest value of the core flux density is 2.15 T during transformer ferroresonance.

Referring back to Fig. 3, an approximate ratio of 2:1:1 exists for the voltages and currents of the three phases, where phases *B* and *Y* are in antiphase with phase *R*, suggesting that all of the three-phase limbs would become highly saturated at the same instant. Moreover, when the line currents of the transformer are added up, borrowing the steady-state convention  $3I_0 = I_R + I_Y + I_B$ , the zero-sequence current  $3I_0$  is not equal to zero, as shown in Fig. 8. This current flows through the neutral as a seventh harmonic with a maximum peak value of 28 A. Acting as the MMF, the flux produced by the three phases’ zero-sequence currents would be in the same direction; this can only mean that the common flux paths would be either the sidelimbs or the tank.

It is worth noting that the transient studies carried out on the transverse view model of Fig. 5 describe the core saturation state. When studying Fig. 7, it is a reasonable approximation to assume that a combination of these conditions applies to the single-limb model of Fig. 4 (2-D axisymmetric model), implying that no significant mutual flux exists and that the limb permeability is mostly low. More specifically, the space average permeability value for each element of the core at each instant has been determined; it was deduced that the lowest value of core limb permeability is 35 at those instants when the ferroresonant currents are at their peak values.

VI. TRANSIENT STUDIES ON THE AXISYMMETRIC MODEL

It should be noted that with a heavily saturated core, neglecting the flux returning via the yokes will give a pessimistically large leakage flux and, thus, a pessimistic value of losses. The axisymmetric model does not attempt to represent the flux in the winding window—it is modeling a section at right angles to the window.

The relative permeability value of 35, deduced from the transient studies in the 2-D transverse view model, has been subsequently employed to set the core permeability in the axisymmetric model. This implies that the core is now linearized at the permeability value corresponding to the highest value of the ferroresonance current, determined in the transverse view model.

Moreover, this axisymmetric model has also been excited by the amp-turn produced on the 400-kV winding's ferroresonant currents of Fig. 3, corresponding to the fundamental sustained mode of ferroresonance.

The tank was modelled to imply that the current induced in it could circulate in other parts of the tank not present in the mesh. This is known as a "global eddy current region" [22]. By contrast, the core frame and the bolts were assumed to carry induced currents which were forced to flow entirely in the component modelled in the mesh. This is true for the core frame, since it has no electrical connection to the corresponding frame on the other side of the yoke. It is also true for the bolts, since they are individual components and electrically insulated from other components.

A quantity of air was modeled between the tank and the mesh boundaries in Fig. 4, to allow for leakage of flux beyond the tank into the surrounding space. The return path for the core flux is through the tank and by leakage paths through the air.

By a way of example, a core bolt was modeled at the centre of the limb, since old transformer designs utilized core bolts instead of insulated bands on the core limb to hold laminations together. Furthermore a bolt structure exists in the gap between the tank lid and the tank wall, spaced at certain intervals in practice. However the 2-D axisymmetric model implies that they are continuous in the third dimension; therefore, a drastically lower value for relative permeability  $\mu_r = 100$  was assigned to this bolt to compensate the approximation imposed on the 3-D structure in the 2-D model.

It is noted that no conductivity was assigned to either the core or the flux shunt in the finite-element analysis, since they are laminated, not bulk materials. However, in order to calculate the losses in the flux shunt, a conductivity of 2.08 MS/m was used for the flux shunt at the stage of postprocessing as will be further detailed.

#### A. Quantification of Losses

Fig. 9 illustrates the flux paths at different instants of ferroresonance. At 1 ms and 5 ms, where the ferroresonant current is not at its peak value, the flux escaping from the core mostly passes through the tank. However at 10 ms, when the ferroresonant current is at its peak value, a significant amount of flux escapes from the core and passes through the nonmagnetic regions, where the T-section core clamping frame, the flux shunt beam, and the tanks tend to have flux concentrations. As far as the flux shunt is concerned, the magnetizing flux leaving the core passes through the laminations in the nonpreferred direction, posing the risk of increased heating.

The finite-element analysis solution was carried out for five cycles (0–0.1 s) to take the average values and to take into account the lower harmonics present in ferroresonant current waveforms. It should be noted that in the simulation, the induced losses in solid (not-laminated) components were calculated at each element in Watts per meter (the length in the third direction), and the total losses were calculated in the postprocessing by integrating the volume losses over the element area and multiplying the assumed peripheral length. In the cylindrical (axisymmetric) solution, this is the average element radius multiplied by  $2\pi$ .

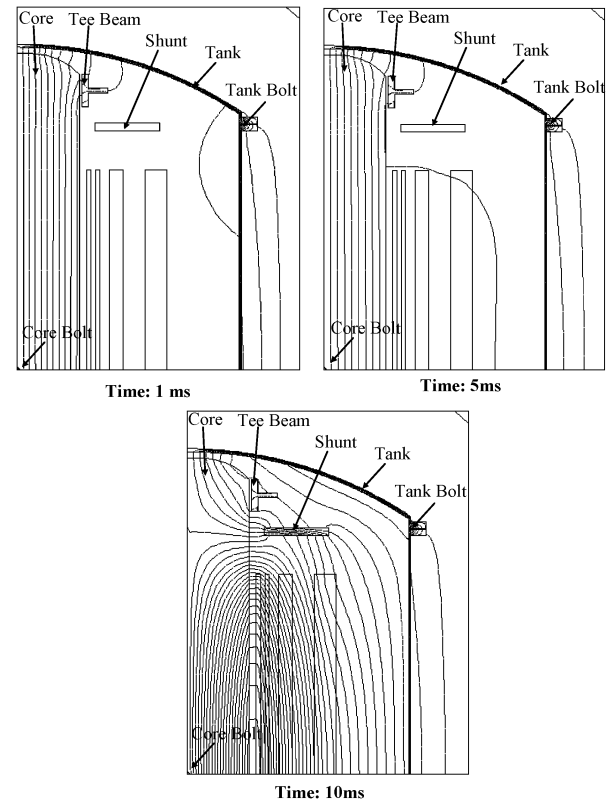


Fig. 9. Flux paths for the core and other parts at different instants of ferroresonance.

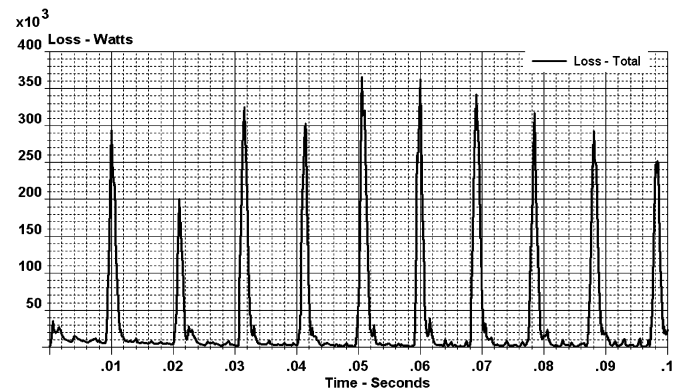


Fig. 10. Variation of total loss with time.

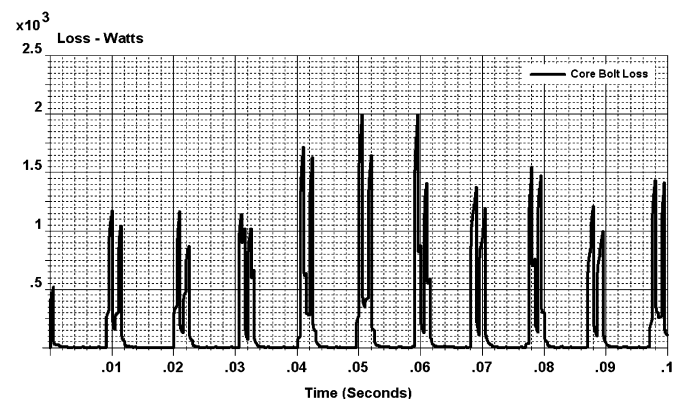


Fig. 11. Variation of core bolt loss with time.

TABLE II  
COMPONENTS' LOSSES ENCOUNTERED DURING FERRORESONANCE ACTIVITY

Parts	Mean loss (Watts)	Apparent volumetric loss density (Watts/cm <sup>3</sup> )
Tank	33563	10
Core frame	3861	36
Tank bolt	17	1.3
Core bolt	420	60

TABLE III  
HARMONIC COMPONENTS OF FLUX DENSITY IN FLUX SHUNT

Frequency	B <sub>x</sub> (mT)	B <sub>y</sub> (mT)
50 Hz	150	5.5
100 Hz	67	1.5
150 Hz	9.8	0.91
200 Hz	7	0.54
250 Hz	2.9	0.34

Fig. 10 illustrates the variation of the total loss with time and Fig. 11 illustrates the loss in the core bolt. The variations of loss with time on the core frame and tank bolt are similar to the ones shown in Figs. 10 and 11.

As seen in Figs. 10 and 11, the peak loss occurs for a short duration corresponding to the peaky ferroresonant current. The overall loss effect may be better assessed through Table II where the mean losses and the apparent volumetric loss density for the components under study are given. "Apparent volumetric loss density" is calculated by using the mean loss divided by the volume of the component.

Although apparent volumetric loss density indicates the overall severity of heating, it is more instructive for any supplementary tangible temperature assessment to utilize the instant loss density (and its variation with time) in each component and, in particular, its distribution when considering skin effect.

### B. Loss Calculation in the Shunt

Due to the fact that the shunt is a laminated structure, the calculation of the ohmic loss directly in the finite-element solution is restricted, unless each lamination is modelled explicitly. This is not possible with the present computational power.

To calculate the losses in a practical manner, it is assumed that any current induced in the shunt laminations would have a negligible effect on the flux density around them. The loss calculation can then be carried out in the postprocessing and based on the magnitude of the flux density impinging on the shunt [26].

Table III tabulates magnitudes of the flux density harmonics obtained by Fourier analyzing the curves of Fig. 12. It is noted that the *y*-component of the flux density is the component parallel to the laminations, and the loss resulting from this component is theoretically available from manufacturer's loss curves. However, the data available from the manufacturer typically start at a flux density of 0.5 T. Therefore, it is assumed that the loss resulting from the flux densities of the order of 5 mT would be negligible.

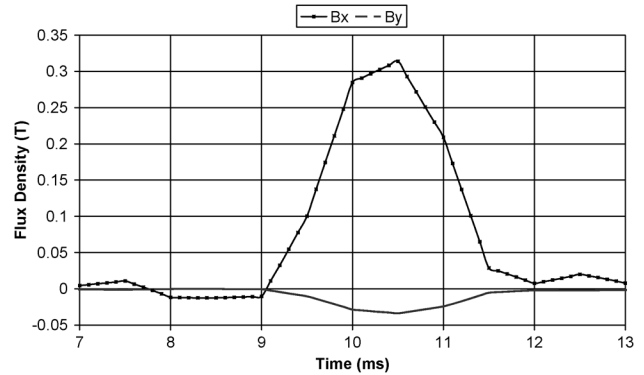


Fig. 12. Variation of flux densities in flux shunt for a quarter of a cycle of ferroresonance.

TABLE IV  
HARMONIC COMPONENTS OF LOSSES IN FLUX SHUNT

Frequency	Loss (kW)
50 Hz	9.3
100 Hz	1.86
150 Hz	0.04
200 Hz	0.021
250 Hz	0.0035

As far as the losses resulting from flux density B<sub>x</sub> (which is the perpendicular component to the lamination) are concerned, (6) was utilized [26]

$$W_e = \frac{2}{3} \times \frac{b^3 \cdot B_o^2 \cdot \omega^2 \cdot F}{\rho} \quad (\text{W/m}^2). \quad (6)$$

$W_e$  describes the loss per unit area (W/m<sup>2</sup>) per lamination,  $b$  is half of the lamination width (in meters),  $B_o$  is the root mean square (rms) value of flux density (T),  $\omega$  is the angular frequency (in radians per second),  $\rho$  is the material resistivity (in ohms per meter), and  $F$  is a multiplying factor.

It is noted that the multiplying factor  $F$  is based on the relationship between lamination thickness and skin depth. This factor is always less than or equal to 1, so by taking it as 1, a pessimistic estimate would be obtained.

In the case of this, transformer  $b$  is 0.025 m and the number of laminations in the shunt is about 1110. Table IV tabulates the losses produced at all harmonic frequencies of B<sub>x</sub>. This results in a shunt mean loss of 11.4 kW and an apparent volumetric loss density of 51.7 W/cm<sup>3</sup>.

### C. Discussion and Interpretation of Losses

With reference to Table II, a special note should be provided for the core bolt, which has the largest apparent volumetric density; constituting itself the most critically affected part. The relative small size of the bolt allows the assessment to be based confidently on just the average losses calculated. It should be kept in mind that in older transformer designs, the main limbs, yokes, and any fourth and fifth limbs are held together with core tie bolts which pass through the whole core stack. These core bolts can pose a particular danger during core saturation events. Heat will be transferred to nearby insulating materials by conduction and convection, increasing the risk of accelerating insulation aging.

Nonetheless, asset-management policies should be aware that if the total energy dissipated in the transformer during ferroresonance is low, then this would have to be very concentrated on a particular part in order to do any damage, whereas a high value of energy would be a major problem wherever the energy is distributed in the flux leakage path during core saturation. It should be reiterated that the figures tabulated in Tables II and III are based on the losses averaged over the whole component and, therefore, cannot provide the exact location of the losses' occurrence. An anatomy map that will reveal regions with concentrated losses can only be achieved either by field measurements or by 3-D finite-element modeling.

Finally, it is highlighted that the results obtained for this case study are very dependent on the accuracy of the  $B-H$  curve employed at high flux densities. There are rarely if ever any measurements at these highly saturated regions, just extrapolations from lower fluxing. Therefore, the losses deduced in this paper provide a comparison of the relative losses in the components, but as absolute values, they must be interpreted with care, bearing in mind the effective length of the components (which can vary for different transformer manufacturers) and the accuracy of the  $B-H$  curve at high flux densities.

## VII. CONCLUSION

This paper presented a 2-D FE transient magnetic study to evaluate the effects of ferroresonance currents on the ohmic losses in structural components of the transformer. The sustained fundamental-mode ferroresonance of a 240-MVA 400/132-kV autotransformer in a double-circuit transmission-line configuration was used in this study.

Even though no 2-D models are adequate to represent EM behaviors of transformer components under transient studies, a set of reasonable approximations has been made in the slim FEA software to allow modeling of the flux distribution and part losses in 2-D transformer models, thus assessing the risk imposed on a transformer due to ferroresonance.

Although ferroresonance is not immediately destructive, the impact on transformers is mainly due to accelerated aging and may be estimated through the power dissipated through ohmic heating during ferroresonance. The losses deduced serve to provide the scope of relative losses in the parts, as for the absolute values, they must be interpreted with care, bearing in mind the effective length of the components.

This paper forms the foundation for more detailed finite-element studies to estimate accompanying temperature rises of the core, structural components, and windings, and eventually to assess the consequential dielectric and thermal impacts on transformer insulation.

## ACKNOWLEDGMENT

The authors would like to express their appreciation to the support provided by AREVA T&D Technology Center, specifically to Dr J.P. Sturgess and Dr A. Sitzia. The technical support provided by National Grid U.K. is also acknowledged.

## REFERENCES

- [1] Y. K. Tong, "NGC experience on ferroresonance in power transformers and voltage transformer on HV transmission systems," in *Inst. Elect. Eng. Colloq.*, 1997, no. 12, pp. 4/1–4/3.
- [2] NGC, Ferroresonance on the Transmission System Tech. Guid. Note TR398 Issue, Dec. 1, 2005 [Online]. Available: [www.national-grid.com/uk](http://www.national-grid.com/uk), Seven Years Statement
- [3] in *Inst. Elect. Eng. Colloq. Warning! Ferroresonance Can Damage Your Plant (Digest No. 1997/349)*, London, U.K., Nov. 12, 1997.
- [4] Y. Li, W. Shi, and F. Li, "Novel analytical solution to fundamental ferroresonance—Part II: Criterion and elimination," *IEEE Trans. Power Del.*, vol. 21, no. 2, pp. 794–800, Apr. 2006.
- [5] W. Piasecki, M. Florkowski, M. Fulczyk, P. Mahonen, and W. Nowak, "Mitigating ferroresonance in voltage transformers in ungrounded MV networks," *IEEE Trans. Power Del.*, vol. 22, no. 4, pp. 2362–2369, Oct. 2007.
- [6] NGC Technical Guid. Note TGN(E)86, Issue, no. 3, Feb. 2005, Control of Ferroresonance Seven Years Statement. [Online]. Available: [www.nationalgrid.com/uk](http://www.nationalgrid.com/uk).
- [7] Slow Transients Task Force of the IEEE Working Group on Modeling and Analysis of Systems Transients Using Digital Programs, "Modeling and analysis guidelines for slow transients—Part III: The study of ferroresonance," *IEEE Trans. Power Del.*, vol. 15, no. 1, pp. 255–265, Jan. 2000.
- [8] J. A. Martinez and B. A. Mork, "Transformer modeling for low- and mid-frequency transients—A review," *IEEE Trans. Power Del.*, vol. 20, no. 2, pt. 2, pp. 1625–1632, Apr. 2005.
- [9] C. Charalambous, Z. Wang, M. Osborne, and P. Jarman, "Validation of a power transformer model for ferroresonance with system tests on a 400 kV circuit," presented at the IPST, Lyon, France, Jun. 4–7, 2007.
- [10] C. Charalambous, Z. Wang, M. Osborne, and P. Jarman, "Sensitivity studies on power transformer ferroresonance of a 400 kV double circuit," *Proc. Inst. Elect. Eng., Gen., Transm. Distrib.*, vol. 2, no. 2, pp. 159–166, Mar. 2008.
- [11] T. Tran-Quoc and L. Pierrat, "An efficient non linear transformer model and its application to ferroresonance study," *IEEE Trans. Magn.*, vol. 31, no. 3, pp. 2060–2063, May 1995.
- [12] J. Pedra, L. Sainz, F. Corcoles, R. Lopez, and M. Salichs, "PSPICE computer model of a nonlinear three-phase three-legged transformer," *IEEE Trans. Power Del.*, vol. 19, no. 1, pp. 200–207, Jan. 2004.
- [13] B. A. Mork, F. Gonzalez, D. Ishchenko, D. L. Stuehm, and J. Mitra, "Hybrid transformer model for transient simulation—Part I: Development and parameters," *IEEE Trans. Power Del.*, vol. 22, no. 1, pp. 248–255, Jan. 2007.
- [14] J. A. Martinez, R. Walling, B. A. Mork, J. Martin-Arnedo, and D. Durbak, "Parameter determination for modeling system transients—Part III: Transformers," *IEEE Trans. Power Del.*, vol. 20, no. 3, pp. 2051–2062, Jul. 2005.
- [15] ATP Rule Book and Theory Book Can/Am EMTP User Group. Portland, OR, 1997.
- [16] J. P. Sturgess, M. Zhu, and D. C. Macdonald, "Finite element simulation of a generator on load during and after a three phase fault," *IEEE Trans. Energy Convers.*, vol. 7, no. 4, pp. 787–793, Dec. 1992.
- [17] M. V. K. Chari, G. Bedrosian, T. J. Sober, and J. Scheibel, "Two dimensional time domain solution of the eddy current problem in rotating electrical machinery," *J. Appl. Phys.*, vol. 67, no. 9, pp. 4714–4716, 1990.
- [18] W. M. Rucker and K. R. Richter, "Calculation of two-dimensional Eddy current problems with the boundary element method," *IEEE Trans. Magn.*, vol. MAG-19, no. 6, pp. 2429–2432, Nov. 1983.
- [19] P. R. Price, "Geomagnetically induced currents effects on transformers," *IEEE Trans. Power Del.*, vol. 17, no. 4, pp. 1002–1008, Oct. 2002.
- [20] SLIM Ver. 3.9.1. AREVA T&D, Stafford, U.K., Oct. 2006.
- [21] A. B. J. Reece and T. W. Preston, *Finite Element Methods in Electrical Power Engineering*. Oxford, U.K.: Oxford University Press, 2000, pp. 16–25.
- [22] J. P. Sturgess, "Two-dimensional finite element modeling of Eddy current problems—The effect of circuit connection," in *Proc. Int. Conf. Electrical Machines*, Manchester, U.K., Sep. 15–17, 1992, vol. 2, pp. 450–452.
- [23] "The Relationship Between Winding Flux Linkage and Average Vector Potential (Amean), Technical Note—Slim Technical Manual," A. Sitzia, Ed., AREVA T&D Technol. Ctr., Stafford, U.K., Jul. 22, 2003.

- [24] "Stacking Factors and Directional Permeabilities in SLIM Magnetic Solvers, *Technical Note—Slim Technical Manual*," A. Sitzia, Ed., AREVA T&D Technol. Ctr., Sep. 13, 2005, Sep. 13, 2005. Stafford, U.K.
- [25] E. Bjerkan, H. K. Hoidalén, and O. Moreau, "Importance of a proper iron representation in high frequency power transformer models," presented at the XIVth I.S.H., Beijing, China, Aug. 25–29, 2005.
- [26] G. W. Carter, *The Electromagnetic Field in Its Engineering Aspects*, 1st ed. White Plains, NY: Longman, 1962, p. 254.



**Charalambos A. Charalambous** (M'08) was born in Nicosia, Cyprus, in 1979.

He received the Class I B.Eng. (Hons.) degree in electrical and electronic engineering and the Ph.D. degree in electrical power engineering from the University of Manchester Institute of Science and Technology, Manchester, Manchester, U.K., in 2002 and 2005, respectively.

Currently, he is a Research Associate within the National Grid High Voltage Research Center at the University of Manchester. His research interests include transformer finite-element modeling, ferroresonance transient studies, and the electrical control and analysis of dc corrosion.

include transformer finite-element modeling, ferroresonance transient studies, and the electrical control and analysis of dc corrosion.



**Zhongdong D. Wang** (M'99) received the B.Eng. and M.Eng. degrees in high-voltage engineering from Tsinghua University, Beijing, China, in 1991 and 1993, respectively, and the Ph.D. degree in electrical engineering from the University of Manchester Institute of Science and Technology, Manchester, U.K., in 1999.

Since 2000 she has been a Lecturer and then became a Senior Lecturer in the School of Electrical and Electronic Engineering at the University of Manchester. Her research interests include transformer modeling, transformer insulation materials, and transformer asset management.

modeling, transformer insulation materials, and transformer asset management.



**Paul Jarman** was born in London, U.K., in 1962. He received the electrical science degree (Hons.) from Cambridge University (Hons.), Cambridge, U.K., in 1984.

He joined the Central Electricity Generating Board, Research Division, where he worked on projects including loss measurement instrumentation for bushings and FRA techniques for transformers. In 1990, he joined the National Grid, Warwick, U.K., as a Transformer Engineer, becoming Head of Transformers in 1998. Since 2001, he has been

the Technical Specialist for transformers within the Asset Strategy Group, National Grid, Warwick, U.K. The group is responsible for technical policy, asset stewardship, and engineering support. He is a chartered electrical engineer and member of the IET.



**Mark Osborne** was born in South Africa in 1969. He graduated from Lancaster University, Lancaster, U.K., with a physics honors degree and received the Ph.D. degree in computer-based analysis of Custom Power Technology' from the University of Sunderland, Sunderland, U.K., in 1997.

He works in the Asset Strategy Group, National Grid, Warwick, U.K. His areas of interest include insulation coordination, substation design, and policy development.